PROCEEDINGS OF SCIENCE

The Design and Status of the HELIX Ring Imaging Cherenkov Detector and Hodoscope Systems

H. B. Jeon,[a] **P. S. Allison,**[b] **M. Baiocchi,**[c] **J. J. Beatty,**[b] **L. Beaufore,**[a] **D. H. Calderón,**[b] **A. G. Castano,**[a] **Y. Chen,**[d] **S. Coutu,**[d] **N. Green,**[e] **D. Hanna,**[f] **S. B. Klein,**[g] **B. Kunkler,**[g] **M. Lang,**[g] **R. Mbarek,**[a] **K. McBride,**[b] **S. I. Mognet,**[d] **J. Musser,**[g] **S. Nutter,**[h] **S. O'Brien,**[f] **N. Park,**[c] **K. M. Powledge,**[a] **K. Sakai,**[a] **M. Tabata,**[i] **G. Tarlé,**[e] **J. M. Tuttle,**[a] **G. Visser,**[g] **S. P. Wakely**[a] **and M. Yu**[d]

[b] *The Ohio State University, Dept. of Physics, Columbus, USA*
[c] *Queen's University, Dept. of Physics, Engineering Physics and Astronomy, Kingston, Canada*
[a] *University of Chicago, Dept. of Physics, Chicago, USA*
[d] *Pennsylvania State University, Dept. of Physics, University Park, USA*
[e] *University of Michigan, Dept. of Physics, Ann Arbor, USA*
[f] *McGill University, Dept. of Physics, Montreal, Canada*
[g] *Indiana University, Dept. of Physics, Bloomington, USA*
[h] *Northern Kentucky University, Dept. of Physics, Geology and Engineering Technology, Highland Heights, USA*
[i] *Chiba University, Dept. of Physics, Chiba, Japan*

E-mail: hyebin@uchicago.edu

HELIX (High Energy Light Isotope eXperiment) is a balloon-borne experiment designed to measure the chemical and isotopic abundances of light cosmic-ray nuclei. Detailed measurements by HELIX, especially of ^{10}Be from 0.2 GeV/n to beyond 3 GeV/n, will provide an essential insight into the propagation processes of the cosmic rays. HELIX features a Ring Imaging Cherenkov (RICH) detector designed to measure the velocity and charge of nuclei with energies greater than ∼1 GeV/n. The RICH detector consists of a radiator volume of high-transparency high-index aerogel tiles imaged by a ∼1 m^2 focal plane instrumented by 200 8×8 arrays of silicon photomultipliers (SiPMs). A scintillating fiber hodoscope read out with SiPM arrays is installed on the top of the RICH radiator plane to improve the accuracy of track reconstruction in the non-bending view of the instrument's magnet spectrometer system. We present the design and current status of the HELIX RICH and hodoscope systems.

38th International Cosmic Ray Conference (ICRC2023)
26 July - 3 August, 2023
Nagoya, Japan

PoS(ICRC2023)121

1. Introduction

HELIX [1] is a balloon-borne experiment to measure the chemical and isotopic abundances of light cosmic-ray nuclei from protons to neon (Z=1-10), especially the ^{10}Be/^{9}Be ratio from 0.2 GeV/n to beyond 3 GeV/n. Be is formed by spallation of heavier cosmic rays in the interstellar medium and decays with a half life of 1.4 Myr which is comparable to the containment time within the Galaxy. Therefore, measurements of the ^{10}Be/^{9}Be ratio can provide an important key for understanding the propagation of cosmic rays.

The HELIX instrument shown in Figure 1 is designed to achieve a mass resolution better than ~3%. The drift chamber tracker (DCT) under a 1 T magnetic field formed by superconducting magnet coils measures the rigidity of incident particles. For particles with energies less than ~1 GeV/n, the top and bottom time-of-flight detectors (TOF) with a distance of ~2.3 m provide velocity measurements and charge measurements at all energies. Velocities of particles with energies exceeding this are obtained by the ring-imaging Cherenkov detector (RICH). A hodoscope located on top of the RICH is employed to reduce the uncertainty in trajectories of particles incident on the RICH in non-bending view of the magnet.

This contribution describes the RICH and hodoscope subsystems and presents their current status and plans. For more details on the HELIX experiment in general [2] and the DCT [3], see these other contributions at this conference.

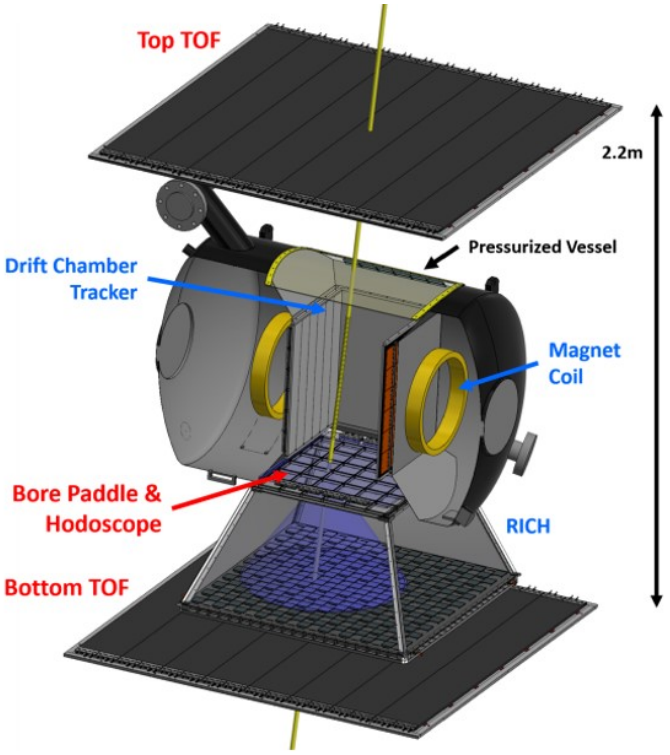

Figure 1: 3D model of the HELIX instrument in a partially-sectioned view with a particle with an energy of ~3 GeV/n going through.

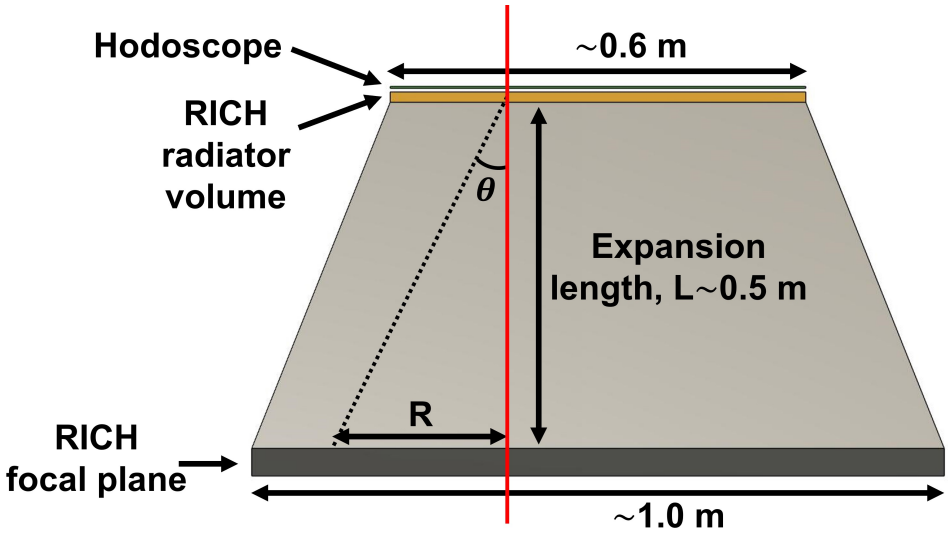

Figure 2: A drawing of the RICH and hodoscope in side view. The red line indicate a particle vertically passing through the RICH. The dashed line shows a cone shape of Cherenkov light with an emission angle of θ produced in the radiator and shining on the focal plane with a radius of R.

2. HELIX Ring-Imaging Cherenkov Detector

The HELIX RICH is a proximity-focused RICH designed to measure the velocity of particles radiating Cherenkov light in a medium by reconstructing rings of photons detected on a focal plane. From the impact parameter of the photon hits from the particle trajectory, the Cherenkov angle can be determined, leading to the particle velocity through the well-known formula

$$\beta = \frac{1}{n \cos\theta}, \tag{1}$$

where β is the particle velocity, n is the refractive index of the medium and θ is the emission angle. To achieve a Lorentz-weighted velocity resolution ($\gamma^2 d\beta/\beta$) of less than 2% up to particle energies of 3 GeV/n, the uncertainty of the refractive index of the radiators must be known to an accuracy on the order of 10^{-4}. It is also essential to know accurately the expansion length between the focal plane and the radiators as well as the precise positions of the SiPMs on the focal plane.

The RICH consists of a radiator volume and focal plane with an expansion length of ~50 cm as shown in Figure 2. In the radiator volume which has an area of 60×60 cm^2, 36 hydrophobic aerogel tiles with dimensions of $10 \times 10 \times 1$ cm^3 are employed. The focal plane with an area of ~1 m^2 comprises 200 custom Hamamatsu silicon photomultiplier arrays (SiPMs), with each 8×8 array of 6×6 mm^2 SiPM containing a total of 6336 micropixels of 75um pitch, populated in a checkerboard pattern shown in the left panel of Figure 3.

The radiators are made with a novel pin-drying process to have high transparency and high refractive index of ~1.15 [4, 5]. A resolution of order 10^{-4} in a refractive index has been achieved for the aerogel tiles satisfying the requirement. The details of the measurements are described in [6–8].

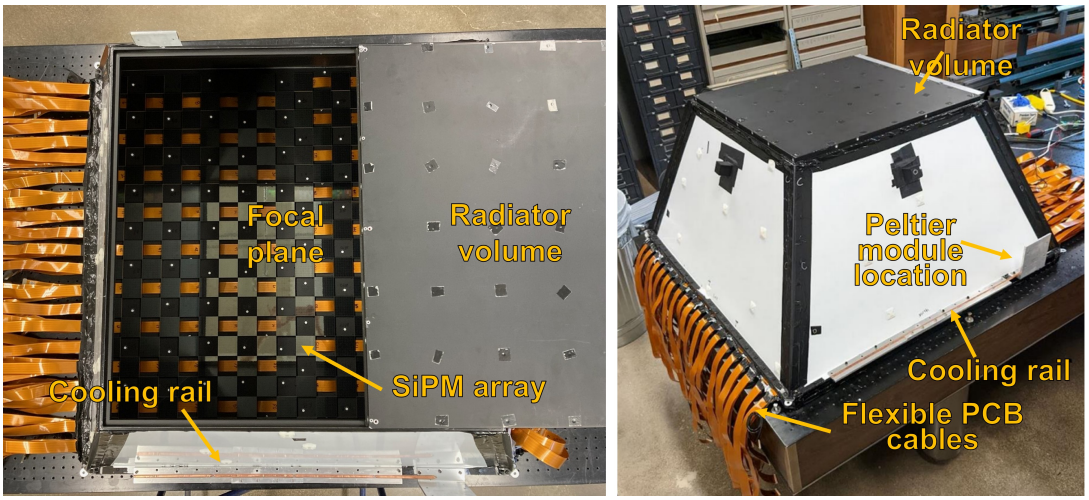

Figure 3: Left: A photo of the top view of the RICH. 200 SiPM arrays are populated on the focal plane in a checkerboard pattern. Right: A photo of the enclosed RICH detector. Flexible cables run from SiPM arrays on the focal plane. The locations of the cooling rail and Peltier module are indicated.

The SiPM arrays are read out by RICH front-end electronics boards through flexible PCB Piezotronics cables with a length of 70 cm pictured in Figure 3. Each RICH front-end board contains 16 CITIROC ASICs [9] with each reading 32 channels to process signals from 8 SiPMs. The CITIROC amplifies the signals and feeds them into two paths of fast and slow shapers generating a timing on an event with a resolution better than 12.5 ns and multiplexed charge output, respectively. On the timing path, an individual discriminator for each channel is used to suppress the dark current noise, while the charge signal is a pulse height determined by a sample-and-hold circuit. The CITIROC can also adjust trim bias voltages for individual channels to optimize the gain of each SiPM. The The trim voltage linearity has been verified, thus the bias voltage applied to an individual SiPM is a sum of the trim voltage for the channel and a common voltage. These are provided by the CITIROC ASIC and the RICH front-end board. A bias on a single SiPM pixel is thus calculated by a sum of the common bias and the corresponding trim voltage.

To control the temperature of the SiPMs, a liquid cooling system is employed consisting of thermoelectric devices, a pump, a radiator and a reservoir. Lower temperatures are desired to suppress dark currents produced by thermal excitation in the sensors and causing random hit noise. To uniformly cool down all SiPMs, two Peltier thermoelectric modules (CP2-127-10-L1-W4.5, Laird Thermal Systems) are placed near two diagonal corners of the focal plane. The colder side of the Peltier modules is thermally connected to ~65 cm-long cooling rails with heat pipes installed along two opposite sides of the focal plane. On the hotter side of the Peltier modules, a heat exchanger is attached to each module to have coolant take heat away. The coolant, HC-40 from Dynalene Inc, absorbs heats from the RICH by circulating through the two heat exchangers in a row and then running into a ~1 L reservoir. The liquid is then pumped by a commercial pump (GJ-N21-DEMSE, Micropump) to a planar radiator with a dimension of 30×30 cm^2 to radiate to space. The chilled coolant then runs through the RICH again and the circulation is repeated. The cooling system is optimized to flow the coolant with a flow rate of 380 mL/min to dissipate the 21 W heat from the RICH out of the instrument.

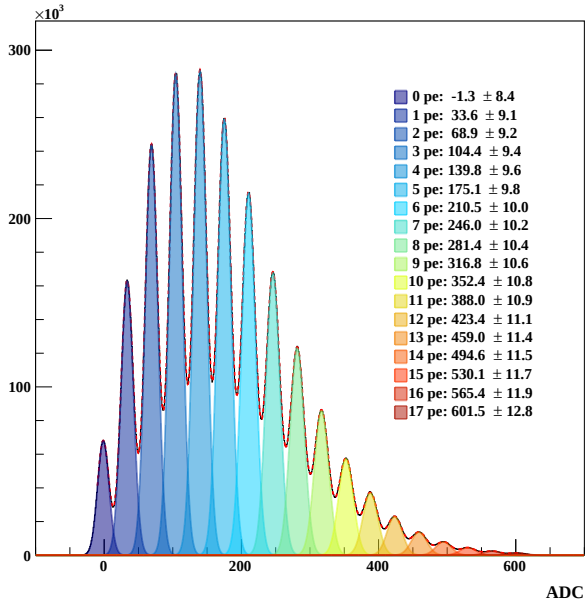

Figure 4: A superposition of photoelectron signals of the gain-matched 12,697 SiPM channels of the RICH focal plane with multiple Gaussian fitting. The noisy channels, 0.8% out of all SiPMs, is excluded in this analysis due to being noisy, dead or controlled by a problematic CITIROC. Clear peak separation with a spacing of ~36 ADC is shown up to 17 photoelectrons (PEs) sensed by SiPM arrays illuminated by a pulsed laser. The legend displays the corresponding number of PEs and mean±sigma of the Gaussian fitting.

To obtain precise measurements of the expansion length, L, and positions of the SiPMs on the focal plane, a Handyscan 307 (CREAFORM) device is used which can rebuild a scanned object as a 3D model with with a 0.025 mm accuracy [10]. Once the focal plane and radiator volume are assembled together but before the placement of sensors and radiators, they are 3D-scanned to determine an accurate expansion L which is crucial for calculating the angle term in Eq.1. The SiPM arrays are then populated to form the focal plane and 3D scanning is carried out again to obtain the exact position of the sensors on the focal plane. The parameter L is found to be 516.6 ± 0.7 from the 3D scan measurements. The measured SiPM 2D positions are consistent with the nominal locations with a residual of -0.1 ± 0.2 mm. The focal plane formed by the top surfaces of the SiPMs is uniform to 0.1 mm.

Gain matching of the SiPMs ensures that every SiPM channel produces the same amount of charge in response to a single photoelectron (PE). The desired SiPM gains are determined by adjusting the common bias and trim voltages. For this purpose, the focal plane is illuminated using a nanosecond pulsed laser diode system (NPL41B, THORLABS) and a fiber cannula diffuser tip (CFDSB05, THORLABS) at the end of the optical fiber. The laser pulse is synchronized using a pulse generator with an external trigger fed to the HELIX data acquisition (DAQ) system. As laser pulses are accumulated, bias voltages are scanned to determine a common voltage that would satisfy all channels in the SiPM array if a trim voltage within the linear range were applied. At the selected common bias, the trim voltage is then scanned in order to fine-tune the bias for individual

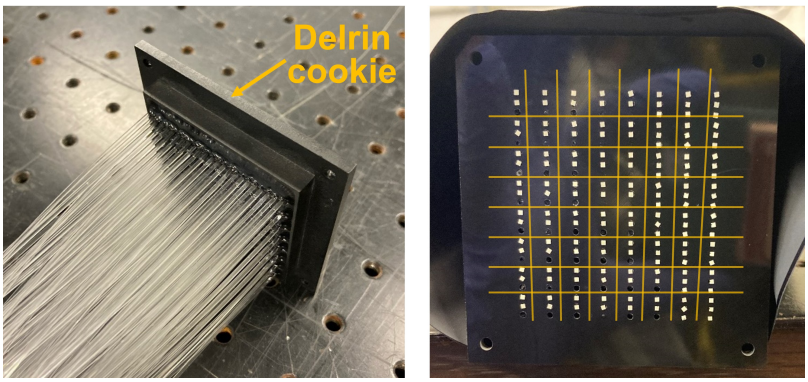

Figure 5: Left: A photo of a Delrin cookie in which a fiber ribbon terminates. Right: A photo of the back side of the Delrin cookie with a multiplexing pattern. The yellow grid lines indicate SiPM pixel channel separations.

channels. This process is possible due to the linearity of the common bias and trim bias that is the bias applied to a SiPM channel can be calculated by adding the common bias to the trim voltage of the respective channel.

Finally, all 200 SiPM arrays are gain-matched from this bias scanning and optimizations. Figure 4 depicts the superposition of the charge distributions of the SiPMs fitted with multiple Gaussian functions implying number of PEs by spacing from the peak of 0 PE distribution. 0.8% out of the SiPMs is excluded because of being noisy, dead or controlled by a problematic CITIROC. The legend in the figure displays the corresponding number of PEs and mean and sigma of the fitting. 99.2% of 12,800 SiPM channels on the focal plane shows remarkable agreement with clear peak separations with a uniform spacing of ~36 ADC, for this gain setting.

3. HELIX Hodoscope

A scintillating fiber hodoscope has been introduced directly above the radiators in order to improve the RICH performance by reducing uncertainties in the trajectories of particles entering the radiators. The hodoscope consists of four 150-fiber ribbons arranged in a single layer. Each ribbon is made of BCF12 plastic scintillating fibers from Saint-Gobain Crystals; each fiber has a 1 mm $\times$ 1mm square cross section and a length of 1 m. The active hodoscope area is 60 cm $\times$ 60 cm covering the full radiator volume. The end of a fiber bundle of the ribbon is woven into a Delrin cookie with a position-multiplexed pattern wherein two or three fibers are assigned to a single SiPM in an 8×8 array. This is necessary because the sensors optically connected with the cookie used for the hodoscope are the same as those used for the RICH. The SiPMs are optically connected with the cookies to sense scintillating light from fibers. The outputs of the SiPM arrays are then read out by the RICH front-end board.

The ribbons are individually wrapped in light-tighting Tedlar sheets. Because the flexible fiber ribbons are not completely colinear, a table must be generated to map 2D fiber positions to channel IDs. This is done by scanning the active area with a ^{90}Sr radioactive source. The measurement system for the mapping is designed to place a source in a desired position, which has a resolution of 1 mm and 50 mm along the X and Y direction, respectively, across the active area, where X

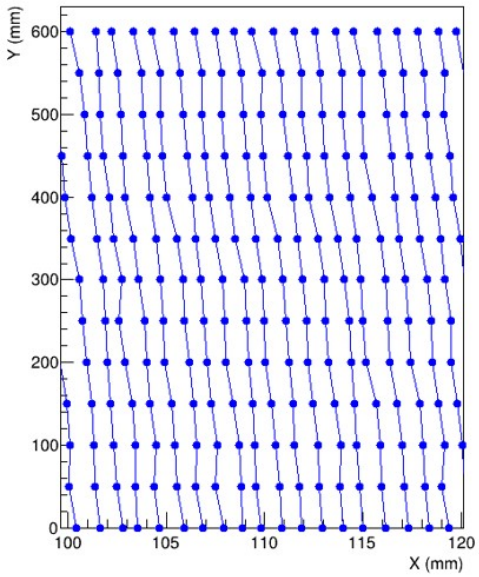

Figure 6: A part of the reconstructed positions of the 600 fibers in the XY plane of the active area of the hodoscope, where the X and Y axes are non-bending and bending directions of the magnet, respectively.

and Y axes are the non-bending and bending axes of the magnet. The fiber fired by the source is found based on the level of signal rates. A map of 600 fibers has been achieved from a total of ~9,000 measurements. Figure 6 shows an example of the reconstructed fibers in the XY plane of the hodoscope.

In addition, a 0.33 mm spatial resolution of the hodoscope is achieved (tentatively) including the uncertainties from intrinsic fiber dimension, the measurement system, the mapping process, and systemic effects. This result implies the hodoscope can improve uncertainties of particle trajectories at the radiators in the non-bending view by a factor of more than 10 compared to that of Monte-Carlo simulations without the hodoscope.

4. Current status and plans

The RICH and hodoscope have been fully assembled and tested. The RICH has been inspected by 3D scanning to determine a precise expansion length and positions of the SiPM arrays on the focal plane. The uniform gains of the 200 SiPM arrays, 12,800 channels in total, across the focal plane has been achieved by adjusting bias voltages for the individual channels. For the hodoscope, as the fibers are not perfectly colinear to each other, more than 9,000 measurements with a radioactive source across the active area have been performed to obtain a map of fiber locations. From the measurements, a preliminary spatial resolution of 0.33 mm has been achieved.

A first HELIX long-duration balloon flight is scheduled for late spring 2024 from Kiruna, Sweden to northern Canada.

References

[1] N. Park *et al.*, in Proc. of the 37th International Cosmic Ray Conference (Berlin) , 091 (2021).

[2] N. Park *et al.*, in Proc. of the 38th International Cosmic Ray Conference (Nagoya) , CRD6 (2023).

[3] McBride *et al.*, in Proc. of the 38th International Cosmic Ray Conference (Nagoya) , PCRD0 (2023).

[4] M. Tabata *et al.*, Nuclear Instruments and Methods in Physics Research Section A **623**, 339 (2010), 1st International Conference on Technology and Instrumentation in Particle Physics (Tsukuba).

[5] P. Allison *et al.*, in Proc. of the 36th International Cosmic Ray Conference (Madison) , 139 (2019).

[6] O'Brien *et al.*, in Proc. of the 37th International Cosmic Ray Conference (Berlin) , 090 (2021).

[7] P. Allison *et al.*, in Proc. of the 36th International Cosmic Ray Conference (Madison) , 133 (2019).

[8] P. Allison *et al.*, Nuclear Instruments and Methods in Physics Research Section A (In Press) (2023).

[9] J. Fleury *et al.*, Journal of Instrumentation **9** (01), C01049.

[10] Creaform handyscan 307, `https://www.creaform3d.com` [Accessed: 2023/07/11].